X-ray study of oil-microemulsion and oil-water interfaces in ternary amphiphilic systems

Dragoslav M. Mitrinović,* Scott M. Williams,† and Mark L. Schlossman‡
University of Illinois at Chicago, Department of Physics, 845 West Taylor Street, Chicago, Illinois 60607
(Received 21 August 2000; published 16 January 2001)

We present x-ray reflectivity and diffuse scattering measurements from the interfaces between oil-rich and microemulsion bulk phases and between oil-rich and water-rich phases in three-component microemulsion systems (consisting of water, alkane, and C_iE_j, where the last represents *n*-alkyl polyglycol ether with $i=4,6,10$ and $j=1,2,4$). The x-ray measurements are analyzed with a two-parameter fit that determines the interfacial roughness, varying from 25 Å to 160 Å, and the interfacial tension, varying from 1.4 mN/m to 0.03 mN/m, for these samples. Although a nonmonotonic profile at the oil-microemulsion interface is not observed, these measurements exclude the presence of oscillating profiles with repeat distances greater then 500 Å.

DOI: 10.1103/PhysRevE.63.021601 PACS number(s): 68.03.Cd, 61.10.Kw, 82.70.Kj, 68.35.Ct

I. INTRODUCTION

Amphiphilic molecules adsorb at water-oil interfaces, reducing the interfacial tension by up to several orders of magnitude. Under favorable conditions, thermodynamically stable dispersions called microemulsions can be formed. They are characterized by the absence of long range order but presence of mesoscopic structure—water and oil domains correlated over distances of hundreds or even thousands of angstroms.

Considerable effort has been placed into studying the structure and behavior of these phases. On the theoretical side the main approaches have been microscopic (often lattice) models, Ginzburg-Landau theories, and membrane theories, and, more recently, density functional theory. For a review of the main results prior to 1994 the reader is referred to Ref. [1]; some of the recent work is discussed in Refs. [2–5].

On the experimental side, it was shown that ternary mixtures of water, oil (typically an alkane), and the nonionic amphiphile C_iE_j [*n*-alkyl polyglycol ether, $H(CH_2)_i(OCH_2CH_2)_jOH$] exhibit all the characteristic features of microemulsions [6]. For a certain range of surfactant concentration (from a few up to 50%, depending upon the amphiphile strength), these systems exhibit a characteristic 2-3-2 reentrant phase behavior, as a function of temperature. At low temperatures, the majority of surfactant is located in the lower, water-rich phase, which is in two-phase equilibrium with the upper, nearly pure oil phase. At high temperatures the picture is inverted; the majority of surfactant is in the upper, oil-rich phase, in two-phase equilibrium with the lower, nearly pure water phase. At intermediate temperatures, the oil-rich and water-rich phases (both nearly pure) are in equilibrium with the third phase, located in the middle of the sample, where the majority of surfactant is intermixed with comparable amounts of water and oil. This middle phase is referred to as a microemulsion. The other two phases, oil-rich and water-rich phases, are throughout the paper occasionally referred to simply as oil and water.

The structure of the microemulsion phase has been extensively studied, as a function of temperature and amphiphilic strength, using small angle neutron scattering (SANS) [7–9], nuclear magnetic resonance [10], and freeze-fracture microscopy [11,12]. SANS studies of microemulsions with strong amphiphiles revealed a scattering peak at nonzero momentum transfer q that is consistent with a real-space correlation function of the form $\sin(k_br)\exp(-r/\xi_b)/(k_br)$, with $k_b=2\pi/d_b$. This correlation function exhibits oscillations of the scattering density corresponding to alternating regions of water and oil separated by sheets of amphiphile, where d_b is a measure of the repeat distance of these internal interfaces. However, little is known about the structure of the external interfaces—those that separate the microemulsion phase from the excess water and oil phases. One of the important predictions of Ginzburg-Landau theories is a quantitative correspondence between structure in the bulk and structure at external interfaces. Layering is expected [13] to occur at these external interfaces, with a repeat distance d_s and correlation length ξ_s equal to the bulk values d_b and ξ_b.

Using neutron specular reflectivity, Zhou *et al.* [14] studied the vapor interface of a one-phase microemulsion consisting of $C_{10}E_4$, water, and octane. They observed surface induced layering with the repeat distance in good agreement with the corresponding bulk length. Using the same system and experimental technique, but this time placing the one-phase microemulsion in contact with a silicon surface, D. D. Lee *et al.* [15] measured a surface repeat distance and correlation length significantly different from the bulk values.

Few direct measurements of the structure at the liquid-liquid interface have been made in these systems. Meunier used ellipsometry to study the structure at the oil-microemulsion and microemulsion-water interfaces of a five-component mixture [16]. He concluded that on the microemulsion side there was a perturbed zone, of thickness comparable with the size of the structure in the bulk. L. T. Lee *et al.* used neutron scattering to study a $C_{10}E_4$ monolayer at the interface between a thin layer of oil (octane) and

*Present address: Motorola, 3850 N. Wilke Road, Arlington Heights, IL 60004.
†Present address: Applied Materials, California.
‡Author to whom correspondence should be addressed. Email address: schloss@uic.edu

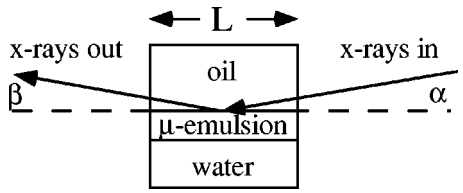

FIG. 1. Experimental geometry.

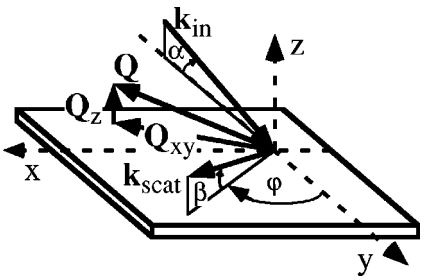

FIG. 2. X-ray scattering kinematics.

water [17]. Their neutron reflectivity data were consistent with an interfacial roughness of 90 Å. Finally, McClain *et al.* [18] used x-ray scattering (reflectivity and diffuse scattering) to study a C_8E_3 surfactant monolayer at the decane-water interface in equilibrium with a small reservoir of middle-phase microemulsion. They found that the x-ray scattering was dominated by capillary waves. The interface was very rough, in agreement with capillary wave theory. However, the water-oil interface is expected to behave differently from the interface between the middle-phase microemulsion and either oil or water—the water-oil interface is predicted to have a simpler structure, with a monotonic density profile, while the other two interfaces are expected to have a structure that correlates with the bulk middle-phase structure.

In this paper, we present direct measurements of the structure of interfaces between a middle-phase microemulsion and the upper oil-rich phase. We used x-ray reflectivity and diffuse scattering to study three different systems: C_4E_1/decane/water, C_6E_2/hexadecane/water, and $C_{10}E_4$/tetradecane/water. The three surfactants used have very different amphiphilic strengths, leading to different structures of the microemulsion phases and different wetting properties. The C_4E_1 microemulsion completely wets the oil-water interface and is weakly structured—SANS measurements show no peak for $q>0$. The C_4E_1 oil-microemulsion interface is expected to have a simple monotonic profile [13]. The C_6E_2 system has more developed structure in the bulk microemulsion phase, with SANS measurements displaying a weak peak for $q>0$, but the middle phase still completely wets the oil-water interface. Finally, in the $C_{10}E_4$ system, the middle phase does not wet the interface between the two excess phases, and SANS measurements show a strong peak at nonzero wave vector q, corresponding to a bulk correlation function dominated by oscillatory behavior. In this case, the oil-microemulsion interface is expected to exhibit layering, consistent with its more developed bulk structure [13].

For each of the three systems we performed x-ray measurements in both two-phase and three-phase regions of the phase diagram. In two-phase samples we studied the interface between the upper, oil-rich phase and the lower, water-rich phase, which we refer to as the oil-water interface. In three-phase samples we studied the interface between the top, oil-rich phase and the middle-phase microemulsion, which we refer to as the oil-microemulsion interface. We demonstrate that in all cases the data are dominated by scattering from capillary waves, and provide values of interfacial tension γ and rms interfacial roughness σ obtained from fits to the data. Our data demonstrate the validity of the capillary wave theory, when combined with the distorted wave Born approximation, for interpreting the x-ray scattering for roughnesses ranging from 25 Å to 165 Å. However, the wave-vector transfer range probed by our experiment was not sufficient to allow definitive conclusions regarding the existence and form of the oscillatory profile at the oil-microemulsion interface.

II. EXPERIMENTAL DETAILS

A. Sample cell and experimental geometry

Figure 1 illustrates the experimental geometry, while the kinematics of surface scattering are illustrated in Fig. 2. The liquids were contained in polycarbonate sample cells with Mylar windows for the x rays [19], sealed with Kalrez O rings from DuPont. The sample cell was placed in a two-stage cylindrical aluminum thermostat with x-ray windows made of Kapton. The thermostat was temperature controlled to $\pm 0.003\,^{\circ}\mathrm{C}$ using Minco adhesive heaters, control thermistors, and Lakeshore 340 temperature controller (the absolute accuracy of the temperature measurement was $\pm 0.3\,^{\circ}\mathrm{C}$).

X rays were incident on the interface at an angle α (note that $\alpha=90°$ is normal to the interface). For arbitrary α, β, and ϕ, the three components of the wave-vector transfer of the scattered radiation $\mathbf{Q}=\mathbf{k}_{\mathrm{scat}}-\mathbf{k}_{\mathrm{in}}$ are

$$Q_x=(2\pi/\lambda)\cos\beta\sin\phi,$$

$$Q_y=(2\pi/\lambda)(\cos\beta\cos\phi-\cos\alpha), \tag{1}$$

$$Q_z=(2\pi/\lambda)(\sin\alpha+\sin\beta),$$

where $\lambda=0.825\pm0.002$ Å is the x-ray wavelength for these measurements. Specular reflection occurs for $\beta=\alpha$ and $\phi=0$ $[Q_x=Q_y=0, Q_z=(4\pi/\lambda)\sin\alpha]$, while for diffuse scattering measurements the outgoing angle β was tuned off the specular condition, but the angle ϕ was kept at the zero value.

The thickness of the upper liquid phase was typically several millimeters and, as indicated in Fig. 1, the primary path of x rays is through the upper liquid phase. The length of this path is a function of the incident and outgoing angles, $L_{\mathrm{upper}}=\frac{1}{2}L(1/\cos\alpha+1/\cos\beta)$, where L is the length of the interface in the direction of the beam (see Fig. 1). For the small angles α and β that were probed in these measurements (all angles $\leqslant 0.3°$), the corresponding variation of the absorption attenuation is less then 1%, and was therefore neglected in the analyses. Most of the measurements were

TABLE I. Sample nomenclature, temperature, number of phases at the given temperature, interface studied (om, oil-microemulsion; ow, oil-water), and sample compositions are given. ν_s, ν_o, and ν_w are volume fractions (at 25 °C) of surfactant, oil, and water.

Sample	System	T (°C)	Phases	Interface	ν_s	ν_o	ν_w
C_4E_1-35	C_4E_1-decane-water	35.0	3	om	0.178	0.661	0.161
C_4E_1-60		60.0	2	ow			
C_6E_2-36	C_6E_2-hexadecane-water	36.0	3	om	0.142	0.484	0.374
C_6E_2-61		61.0	2	ow			
$C_{10}E_4$-38-0	$C_{10}E_4$-tetradecane-water	38.0	3	om	0.048	0.476	0.476
$C_{10}E_4$-38-1		38.0	3	om			
$C_{10}E_4$-38-3		38.0	3	om			
$C_{10}E_4$-33		33.3	2	ow			

taken using a sample cell with $L=75$ mm, although in several cases a smaller cell, with $L=25$ mm, was used. Using a shorter x-ray path length through the upper phase is advantageous due to reduced absorption and background bulk scattering, but places more stringent requirements on the vertical size of the incident x-ray beam. For accurate measurements, the x-ray beam's footprint L_f, which depends on the beam's vertical size D and incident angle α, $L_f=D/\sin\alpha$, must be smaller then the size of the interface L. We found that in most cases $L=75$ mm was a more practical choice than $L=25$ mm. However, due to high absorption in the lower phase, the smaller sample cell with $L=25$ mm was used for measuring the bulk scattering from the lower phase (see Sec. II C).

To set the incident beam size and vertical divergence, two slits placed approximately 60 cm apart were used prior to the liquid sample. The slit gaps were typically 5 to 10 μm in the vertical, and 10 mm in the horizontal direction [the beam size (full width at half maximum) before the slits was approximately 0.5 mm$\times$2 mm, vertical $\times$ horizontal]. Following these two slits, but prior to the sample, a scintillator monitor was used to measure the incident beam flux. The sample was followed by a slit with a vertical gap of 0.1 to 0.5 mm, to reduce the background scattering (mainly parasitic scattering from the slit immediately preceding the sample), and the scintillator detector was preceded by a slit with a vertical gap of 0.1 to 0.6 mm, which set the detector resolution. Both slits that followed the sample had horizontal slit gaps of 20 mm.

B. Materials and procedures

Table I lists the sample nomenclature and compositions. $C_{10}E_4$ (tetraethylene glycol mono *n*-decyl ether) was purchased from Nikko Chemicals (distributed by Barnet Products); C_6E_2 (diethylene glycol monohexyl ether, 98+%) and C_4E_1 (2-butoxyethanol, 99.8+%) were purchased from Fluka. Tetradecane (99+%) and hexadecane (99%) were obtained from Aldrich; decane (99+%) was purchased from Sigma. All these chemicals were used as received. High purity water was produced from a Barnstead NanoPure system.

A teflon coated stir bar was used to stir the samples to speed up the thermal equilibration. After each change of temperature samples were stirred vigorously for a brief period of time to intermix the materials, followed by a long period of very slow stirring to bring the sample to thermal equilibrium. The sample was judged to be in equilibrium if the bulk phases and interface were visually clear and if the x-ray scattering from the interface was stable over a period of several hours. The total amount of time required to equilibrate the sample varied from a few hours for C_4E_1 up to 2 days for $C_{10}E_4$.

Once the sample equilibrated, x-ray scattering was measured. Two types of measurement, diffuse scattering and reflectivity, were made by fixing the incident angle α while scanning the angle β. These β scans were repeated for a series of values of the incident angle α. The difference between the two types of measurement was in the range of β motion. For the reflectivity, the width of the β scan was typically a few times the width of the specular peak itself (which is primarily determined by the size of the detector slits). The diffuse scattering was taken using wide, high statistics β scans, which included both the surface enhancement peak, at β equal to the critical angle θ_c, and the specular peak at $\beta=\alpha$. This procedure differs somewhat from that usually used at the liquid-vapor interface. There, reflected intensity at the given Q_z is determined by measuring the scattered intensities at $\mathbf{Q}=(0,0,Q_z)$, $(0,+\Delta Q_y,Q_z)$, and $(0,-\Delta Q_y,Q_z)$. The average of the two off-specular measurements then determines the background level, which is subtracted from the measurement at the specular position to determine the reflected intensity. While this method was successfully used at liquid-vapor interfaces [20], we found that β scans were more convenient at liquid-liquid interfaces, where the background is often dominated by bulk scattering from the upper liquid phase. For fixed α and β, this background is roughly proportional to the incident beam's path length through the upper phase, which depends on the precise position where the x-ray beam hits the interface. Although we always try to position the x-ray beam at the center of the flat portion of the interface, some variations occur due to limited accuracy of mechanical motions of the spectrometer. Therefore, a more consistent measure of the background is obtained in β scans, where the beam position at the interface is fixed during the scan, than in Q_y scans, where both input arm and sample must be moved during the scan [20].

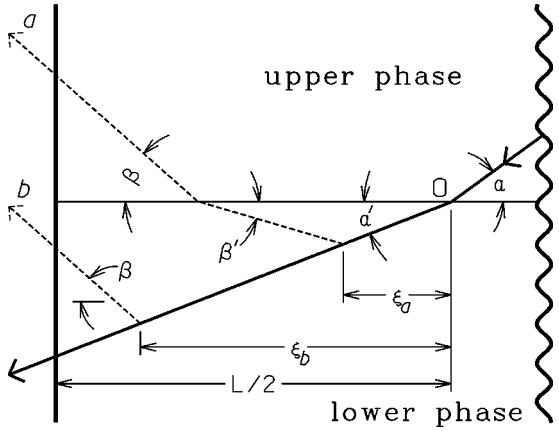

FIG. 3. Two types of scattering from the lower phase are illustrated. The magnitudes of all angles are greatly exaggerated ($\alpha,\alpha',\beta,\beta'<0.15°$). Interface has size L. Beam is assumed to hit the interface at its center, at distance $L/2$ from either of the two edges. Only one-half of the interface is shown in the figure.

A reflectivity close to 100% was measured below the critical angle θ_c for the total reflection of x rays from the interface. As α was increased above the critical angle the reflectivity dropped rapidly.

All x-ray measurements were conducted using the liquid surface spectrometer at the X19C beamline, at the National Synchrotron Light Source, Brookhaven National Laboratory. Beamline setup and experimental procedures are described in more detail elsewhere [20].

C. Background determination and subtraction

In addition to surface scattering (specular reflection and diffuse scattering), scattering from both bulk phases (separated by the interface studied) was observed. For all the diffuse scattering data presented, this bulk scattering was measured, calculated, and subtracted before the data were analyzed.

The relative intensities of the bulk scattering from the upper and lower liquid phases depended upon the location within the phase diagram of the sample studied. For samples in the three-phase region, backgrounds from the upper and the lower phases (oil-rich phase and middle-phase microemulsion) were of comparable intensity, and both were taken into account. The exception is the C_6E_2 sample at 36 °C, where, at the incident angles for which the diffuse scattering data were taken, background was much smaller than the surface signal and was therefore not measured, but instead a small constant background was used in the data analyses. The two-phase region samples of the C_4E_1 and C_6E_2 systems were studied at temperatures above the three-phase region, where most of the surfactant is located in the upper, oil-rich phase. For these samples, we found that background scattering from the lower, water-rich phase is negligible in comparison with the scattering from the upper phase, and therefore only the latter was taken into account. However, the two-phase sample of the $C_{10}E_4$ system was studied at a temperature below the three-phase region where most of the surfactant is located in the lower, water-rich phase. Here, the bulk scattering backgrounds from the two liquid phases were comparable and both were taken into account.

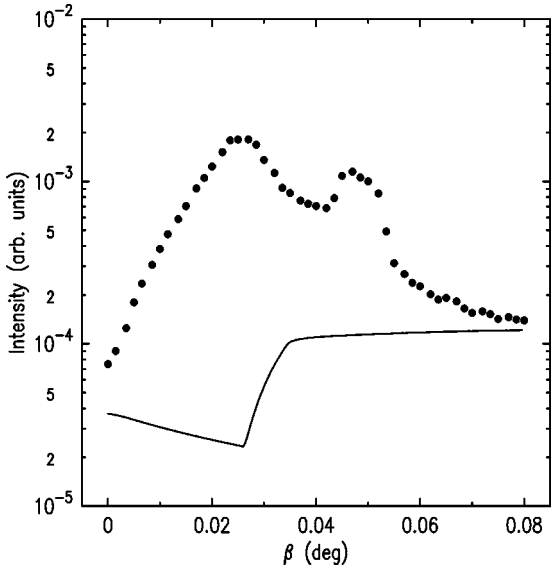

FIG. 4. Raw data taken at $\alpha=0.051°$ (dots), and calculated background from the lower phase (line), for the $C_{10}E_4$-38-1 sample. Peak at lower β is the surface enhancement, while that at higher β is specular reflection.

The procedure for the measurement and determination of the background bulk scattering differed for the upper and lower phases. Background from the upper phase was measured immediately after each of the diffuse scattering β scans by lowering the interface below the x-ray beam and repeating the same scan. Scattering measured in that way was multiplied by $\frac{1}{2}$ to compensate for the fact that in this case the path of the unscattered beam through the upper phase, and thus the bulk scattering which is proportional to it, is twice as large as in the case when the beam hits the center of the interface. Here, only single scattering events are taken into account and we also assume that nearly all of the beam is transmitted through the interface, with only a small fraction being reflected. This is justified in all cases where background scattering from the upper phase was significant.

Bulk scattering from the lower phase is more complicated, and cannot be measured in such a direct way. Figure 3 illustrates two kinds of scattering from the lower phase—ray *a* reenters the upper phase before leaving the sample, while ray *b* is scattered from the lower phase straight into the air. Scattering from the lower phase can be calculated in terms of the experimentally measured scattering probability per unit length of the main beam path through the lower phase. The details of the calculation are given in the Appendix. Figure 4 shows an example of the background from the lower phase for a $C_{10}E_4$ sample at 38 °C, together with the raw β scan taken at $\alpha=0.057°$. The background from the upper phase was negligible in this case. The sharp feature in the background near the critical angle is due to reentrant scattering (e.g., ray *a* in Fig. 3) being permitted only for $\beta>\theta_c$.

III. SCATTERING THEORY

In the spirit of a hybrid model of capillary wave theory [21], we describe a liquid-liquid interface in terms of an

intrinsic electron density profile normal to the interface, $\rho_e(z)$, which is then roughened by capillary fluctuations. To describe the latter, we use the height-height correlation function, defined as $C(r)=\langle h(0)h(r)\rangle$, where $h(r)$ is the local interfacial height above the mean interfacial plane, and r is the distance between two points on the interface. The correlation function $C(r)$ is given by [18,22]

$$C(r)=\frac{k_BT}{2\pi\gamma}K_0\left[\left(\frac{g\Delta\rho}{\gamma}(r^2+r_0^2)\right)^{1/2}\right], \tag{2}$$

where $K_0(x)$ is the modified Bessel function of the second kind, g is the gravitational acceleration, γ is the interfacial tension, $\Delta\rho$ is the mass density difference between the two phases, and r_0 is a small length scale cutoff introduced to ensure a finite value of the rms interfacial roughness $\sigma \equiv\sqrt{C(0)}$. The origin of this cutoff is microscopic, and at present there is neither theoretical nor experimental consensus on the proper choice of r_0.

Using the distorted wave Born approximation, interfacial x-ray scattering can be written as a sum of the specular and diffuse scattering [22]. The former is given by

$$I_{\rm spec}=I_0\left|\frac{Q_z-Q_z^t}{Q_z+Q_z^t}\right|^2|\Phi(\sqrt{Q_zQ_z^t})|^2\exp(-Q_zQ_z^t\sigma^2). \tag{3}$$

Here, I_0 is the incident intensity, Q_z^t is the z component of the momentum transfer with respect to the lower phase, given in terms of α and β as

$$Q_z^t\equiv\frac{2\pi}{\lambda}(\sqrt{\alpha^2-\theta_c^2}+\sqrt{\beta^2-\theta_c^2}) \tag{4}$$

(at the specular condition, $\alpha=\beta$), θ_c is the critical angle for total reflection, and $\Phi(q)$ is the Fourier transform of the derivative of the intrinsic electron density profile, normalized to the electron density difference $\Delta\rho_e$ between the two bulk phases $(\rho_{e,\rm lower}-\rho_{e,\rm upper})$,

$$\Phi(q)=\frac{1}{\Delta\rho_e}\int dz\,\frac{d\rho_e(z)}{dz}\exp(iqz). \tag{5}$$

The diffuse scattering is given by

$$I_{\rm diff}=\frac{I_0}{\sin\alpha}\frac{Q_c^4}{256\pi^2}\int d\beta\,d\phi|T(\alpha)|^2|T(\beta)|^2|\Phi(\sqrt{Q_zQ_z^t})|^2 \times\frac{\exp[-{\rm Re}(Q_z^t)^2\sigma^2]}{|Q_z^t|^2}\int d^2r(e^{|Q_z^t|^2C(r)}-1)e^{i\mathbf{Q}_{xy}\cdot\mathbf{r}}. \tag{6}$$

Here, $\mathbf{Q}_{xy}$ is the two-dimensional in-plane momentum transfer vector whose two components Q_x and Q_y are given by Eq. (1), Q_c is the critical momentum transfer for total reflection, $Q_c=(4\pi/\lambda)\sin\theta_c$, and $T(\alpha)$ and $T(\beta)$ are the Fresnel field (amplitude) transmission coefficients for an ideal, sharp interface [23].

Integration over β and ϕ corresponds to the angular acceptance range of the instrument (resolution volume) determined by the detector slits. For a coarse resolution in the horizontal direction, integration can be done analytically over all angles ϕ, in which case the above expression simplifies to

$$I_{\rm diff}=\frac{I_0\lambda}{\sin\alpha}\frac{Q_c^4}{256\pi^2}\int d\beta|T(\alpha)|^2|T(\beta)|^2|\Phi(\sqrt{Q_zQ_z^t})|^2 \times\frac{\exp[-{\rm Re}(Q_z^t)^2\sigma^2]}{|Q_z^t|^2}\int dy(e^{|Q_z^t|^2C(|y|)}-1)e^{iQ_yy}, \tag{7}$$

where Q_y is given by Eq. (1) with $\phi=0$.

We would like to make a few comments regarding the diffuse scattering formalism used in the analysis of the data. First, Eq. (6) was derived in Ref. [22] under the assumption that $Q_c\sigma$ is small. For the roughest of our samples, $Q_c\sigma$ reaches a value as high as 1.4, and it is possible that the corresponding error is non-negligible. Unfortunately, neither the error estimate nor a better formalism is currently available in the literature. Second, several recent papers [24,25] used the diffuse scattering formalism with the differential cross section $d\sigma/d\Omega\propto|T(\alpha)|^2|T(\beta)|^2Q_{xy}^{\eta-2}$, where η is a dimensionless quantity defined as $\eta=Q_z^2k_BT/(2\pi\gamma)$. In this approximation, true specular reflection does not exist, but instead the diffuse scattering has a cusp singularity at $Q_{xy}=0$. This is a consequence of a logarithmic approximation for the height-height correlation function, $C(r)\approx A+B\log(r)$, so that $C(r)$ diverges logarithmically for large r instead of having exponential decay as in Eq. (2). This approximation for $d\sigma/d\Omega$ can be successfully used instead of Eq. (7) provided that (a) the experimental resolution $\Delta Q_y\approx(2\pi/\lambda)\beta\Delta\beta$ is coarse enough, $\Delta Q_y\gg(\Delta\rho_mg/\gamma)^{1/2}$, so that the experiment is not sensitive to the form of $C(r)$ for large r, and (b) at least one of the two angles α and β is always much greater than θ_c, so that the distinction between Q_z and Q_z^t need not be made. Condition (a) is generally very well satisfied in most measurements found in the literature. In our experiment, due to small angles and low values of interfacial tension, values of ΔQ_y and $(\Delta\rho_mg/\gamma)^{1/2}$ are comparable. More importantly, condition (b) is not satisfied in our experiment. Therefore, Eq. (6) is more appropriate for the analysis of our data than this logarithmic approximation.

The approximation of infinitely coarse resolution in the horizontal direction, made in deriving Eq. (7) from Eq. (6), also deserves a brief discussion. Using the $d\sigma/d\Omega\propto Q_{xy}^{\eta-2}$ result mentioned above (this is justified for the rough error estimate to be made) it can be shown [19], for $\eta<1$, that the relative error ϵ of a diffuse scattering calculation, made when replacing a finite horizontal angular acceptance $\Delta\phi$ by an infinite value, is

$$\epsilon\approx\frac{1}{2-\eta}\left(\frac{\Delta\phi/2}{|\cos\beta-\cos\alpha|}\right)^{\eta-1}. \tag{8}$$

For $\eta>1$, replacing $\Delta\phi$ by an infinite value is not acceptable. However, the presence of a small length scale cutoff r_0 in Eq. (2) modifies the large Q_{xy} behavior of the differential cross section—for $Q_{xy}>r_0^{-1}$, $d\sigma/d\Omega$ decays much faster than $Q_{xy}^{\eta-2}$. The maximum Q_{xy} probed by the experiment is set by $Q_{x,\max}\approx(2\pi/\lambda)\sin(\Delta\phi/2)$. Therefore, for $\Delta\phi \gtrsim \lambda/(\pi r_0)$, the assumption of infinitely coarse resolution is valid regardless of the value of η; otherwise Eq. (8) must be used to estimate the error. In the data analysis presented here, the relative error in the calculation of diffuse scattering, associated with setting $\Delta\phi=+\infty$, was always less than 1%.

IV. DATA AND ANALYSIS

For the angle of incidence α fixed at some value above the critical angle θ_c, diffuse scattering as a function of β exhibits two peaks—one, due to the $|T(\beta)|^2$ term, at $\beta=\theta_c$, and another at the specular condition $\beta=\alpha$ (see, e.g., Fig. 6 below). For a typical instrumental resolution, the latter peak cannot be resolved from the true specular reflection peak. Therefore the quantity of experimental interest is the *effective reflectivity*, defined here as the difference in scattered intensity between the specular condition and the background level, determined by offsetting the angle β from the specular position as discussed in Sec. II B. By repeating this measurement for a series of values of α one obtains the experimental effective reflectivity curve (see Fig. 9 below). This curve can then be compared with the calculated effective reflectivity, which depends on both σ and γ.

One approach to calculation of the effective reflectivity is to use Eq. (3), with σ replaced by $\sigma_{\rm eff}$, the latter being a function of instrumental resolution and angle of incidence [24,26–28]. We use a slightly different approach. For each β scan representing a single effective reflectivity measurement, we calculate the sum of diffuse scattering and specular signal using Eqs. (3) and (7) over the same range of β as the measurement. Then, we determine and subtract the background level in the same way as was done for the actual experimental data. This approach, although essentially equivalent to the aforementioned one, has the advantage that the somewhat arbitrary choice of the data points (in the wings of the peak at the specular position) used to determine the background level does not influence the data analysis.

Data were analyzed using the following procedure. First, low Q_z reflectivity data were analyzed using Eq. (3) to determine the critical wave-vector transfer Q_c. Then, an iterative procedure was used to fit reflectivity and diffuse scattering, using interfacial tension γ and roughness σ as the only two fitting parameters. Each iteration consisted of fitting the effective reflectivity data, using σ as the fitting parameter, followed by fitting diffuse scattering β scans, using γ as the fitting parameter. After several iterations, values of σ and γ would stabilize. However, in the case of $C_{10}E_4$ data, due to the very high roughness, the specular peak disappeared so rapidly as a function of Q_z that measuring reflectivity and diffuse scattering separately was not practical (see Fig. 8 below). In this case all the data consist of full β scans with both the surface enhancement and specular peaks, and were fitted to both σ and γ simultaneously. The cutoff r_0 was calculated for each pair of values γ and σ by solving Eq. (2) for r_0 and using $\sigma^2=C(0)$.

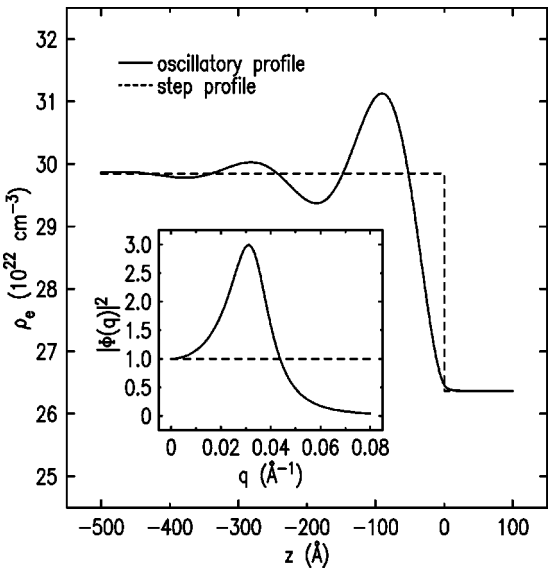

FIG. 5. Oscillatory electron density profile at the oil-microemulsion interface (full line) and step profile (dashed line), as a function of the z coordinate normal to the interface ($z>0$ corresponds to oil phase). Oscillatory profile is based on Refs. [13] and [29], and is calculated here using the microemulsion repeat distance $d_s=191$ Å and microemulsion correlation length $\xi_s=97$ Å. In the inset, the properly normalized Fourier transform of the derivative of the electron density is shown for both the oscillatory (full line) and the step function profile (dashed line).

Data for all interfaces were analyzed using the sharp, steplike intrinsic profile $\rho_e(z)$, for which $\Phi(q)=1$. Data for the oil-microemulsion interface for $C_{10}E_4$ microemulsions were also analyzed using an oscillatory interfacial profile, calculated by Gompper and Schick [13,29]. This profile is parametrized by four lengths—the repeat distance d_s and the exponential decay (correlation) length ξ_s on the microemulsion side of the interface, and two correlation lengths on the oil side of the interface. The latter two do not influence the profile significantly as long as they are much shorter than the characteristic microemulsion lengths (values of 4 Å and 6 Å were used in the calculation). The theory predicts that these interfacial lengths, d_s and ξ_s, are equal to the bulk lengths d_b and ξ_b. The latter were measured by Sottmann *et al.* using small angle neutron scattering [9], $d_b=191$ Å and $\xi_b=97$ Å. This oscillatory electron density profile is shown in Fig. 5, and the corresponding Fourier transform $\Phi(q)$ is shown in the inset.

Our results are summarized in Table II, where values of Q_c, γ, σ, and r_0 are given for each of the samples [30]. For the $C_{10}E_4$ microemulsion at 38 °C, values of the fitting parameters, γ and σ, are shown for both step-like and oscillatory profiles.

Figure 6 demonstrates the diffuse scattering data (dots) and fits to the data (full lines) for the C_4E_1 system at (a) 35 °C (oil-microemulsion interface) and (b) 60 °C (oil-water interface). Each of the curves is labeled on the plot by the value of the incident angle α. The peak to the left, known as

TABLE II. Experimental results summarized. Interfacial tension γ and roughness σ are fitting parameters, while cutoff r_0 is calculated from γ and σ as explained in the text. Also specified are the measured values of the critical wave-vector transfer Q_c, type of interfacial profile used in the fitting (oscillatory or step profile), and interface studied [oil-microemulsion (om) or oil-water (ow)]. Where measured, the absorption lengths for x rays in the upper (l_u) and lower (l_l) phases are also given.

Sample	Interface	Q_c (Å^{-1})	Profile	γ (mN/m)	σ (Å)	r_0 (Å)	l_u (mm)	l_l (mm)
$C_{10}E_4$-38-0	om	0.0084±0.0004	step	0.033±0.007	150±3	5–200	18.8	8.6
			osc	0.034±0.007	155±3	1–80		
$C_{10}E_4$-38-1	om	0.0081±0.0004	step	0.030±0.006	139±2	90–1000	18.8	8.6
			osc	0.031±0.006	144±2	30–500		
$C_{10}E_4$-38-3	om	0.0082±0.0004	step	0.034±0.007	164±3	0.3–30	18.4	8.9
			osc	0.034±0.007	168±3	0.1–13		
$C_{10}E_4$-33	ow	0.0096±0.0004	step	0.058±0.009	108±1	25–300	17.2	6.9
C_6E_2-36	om	0.0079±0.0004	step	0.27±0.03	54.8±0.7	5–150		
C_6E_2-61	ow	0.0088±0.0004	step	1.0±0.1	29.1±0.1	25–600		
C_4E_1-35	om	0.0078±0.0004	step	0.22±0.03	61.7±0.9	3–150	14.9	9.3
C_4E_1-60	ow	0.0110±0.0004	step	1.4±0.2	26.0±0.2	4–80	18.5	6.4

the surface enhancement or Yoneda peak, always occurs at the same β corresponding to the critical angle θ_c. The other peak, which progressively shifts to the right, occurs at the specular position $\beta=\alpha$, and represents a combination of the true specular reflection and the diffuse scattering peak at the specular position. The widths of both peaks are primarily determined by the size of the detector slits. For example, all β scans shown in Fig. 6(a) were taken with the detector slit gap of 0.2 mm. In Fig. 6(b), scans at $\alpha=0.078°$ and $\alpha=0.117°$ were taken with the slit gap of 0.1 mm, while the scan at $\alpha=0.097°$ was taken with the detector slit gap of 0.16 mm.

Figure 7 demonstrates the diffuse scattering data and fits for the C_6E_2 system at (a) 36 °C (oil-microemulsion interface) and (b) 61 °C (oil-water interface). The data for the $C_{10}E_4$ system at (a) 38 °C (oil-microemulsion interface) and (b) 33.3 °C (oil-water interface) are shown in Fig. 8.

The effective reflectivity from all the samples is shown together in Fig. 9, where calculated Fresnel reflectivities (for ideal, smooth interfaces) are also shown (dashed curves).

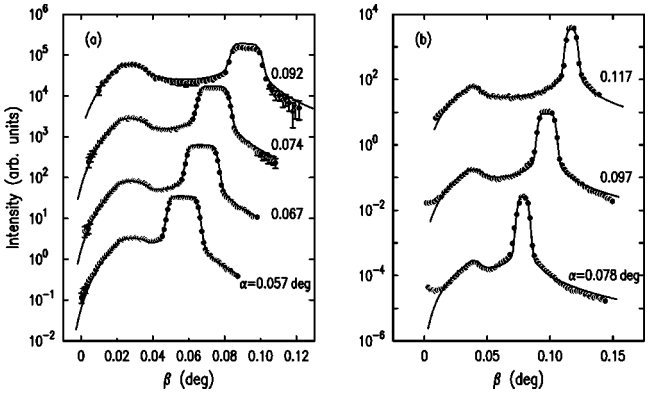

FIG. 6. Diffuse scattering for C_4E_1 microemulsion system. For each of the diffuse scattering curves, also given is the incident angle α in degrees. (a) Oil-microemulsion interface at 35 °C. (b) Oil-water interface at 60 °C.

V. DISCUSSION

Scattering data of the type presented here can provide a measure of the interfacial tension and roughness, as well as the form of the intrinsic electron density profile normal to the interface. In this section we discuss, in turn, each of these aspects of the interface.

First, we note that good agreement between the data and the fits demonstrates that capillary wave theory, combined with the distorted wave Born approximation, is sufficient to quantitatively describe the scattering from all the samples studied. The discrepancies between the data and fits at low β, particularly visible in Figs. 6(b) and 7(b), is believed to be due to scattering from the curved part of the interface near the downstream (with respect to the beam) edge of the sample. The discrepancies at high β (to the right of the specular peak) in the top two curves in Fig. 8(b) are due to underestimated background from the lower phase. Our background subtraction procedure, explained in Sec. II C, generally worked well. However, in these two cases the calculated background was too low.

These interfaces span a wide range of interfacial tension from 0.03 mN/m to 1 mN/m. The tensions shown in Table II

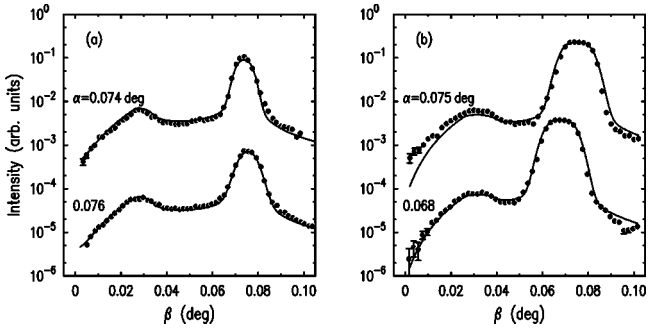

FIG. 7. Diffuse scattering for C_6E_2 microemulsion system. For each of the diffuse scattering curves, also given is the incident angle α in degrees. (a) Oil-microemulsion interface at 36 °C. (b) Oil-water interface at 61 °C.

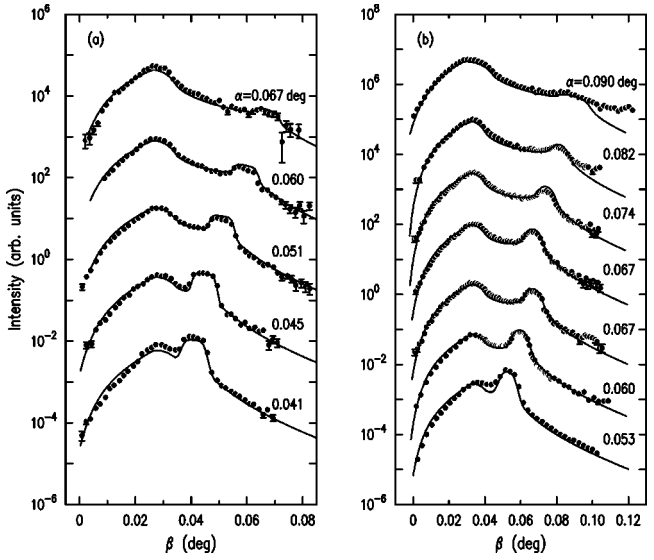

FIG. 8. Diffuse scattering for $C_{10}E_4$ microemulsion system. For each of the diffuse scattering curves, also given is the incident angle α in degrees. (a) $C_{10}E_4$-38-1 (oil-microemulsion interface at 38 °C). (b) $C_{10}E_4$-33 (oil-water interface at 33 °C).

illustrate two trends. The $C_{10}E_4$-tetradecane-water system exhibits much lower tensions than the other two systems, consistent with the expectation that the longer chain $C_{10}E_4$ is a much stronger amphiphile than either C_6E_2 or C_4E_1. Also, the tensions for the oil-microemulsion interface in the three-phase region are smaller than for the oil-water interface in the two-phase region of the same system. This result is reasonable for the two wetting systems C_4E_1 and C_6E_2 in which the microemulsion phase wets the oil-water interface, for the following two reasons. First, for the wetting systems, $\gamma_{om}+\gamma_{mw}<\gamma_{ow}$ (where γ_{ab} stands for the interfacial tension of the *a*-*b* interface, *o* for oil, *w* for water, and *m* for microemulsion). Second, for these systems it is also known that γ_{ow} in the three-phase region is smaller than γ_{ow} in the nearby two-phase region [4]. For the $C_{10}E_4$ system our result is consistent with the expectation that the structured microemulsion phase will reduce the tension with a neighboring oil or water phase beyond the reduction expected from a simple monolayer present at the oil-water interface [1].

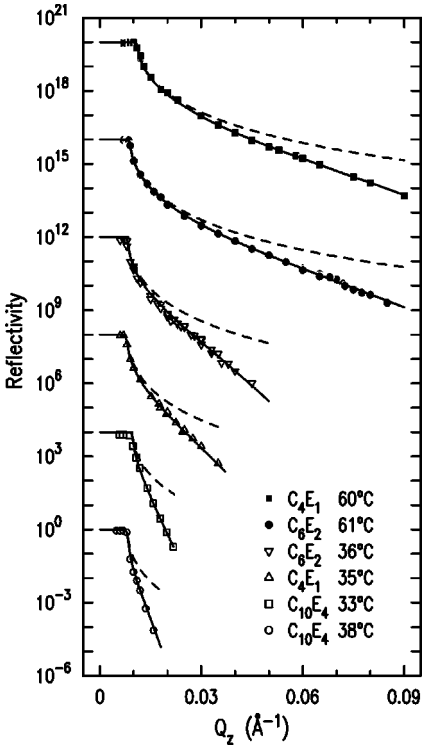

FIG. 9. Reflectivity for all the samples. Full lines are fits to the data, while dashed lines are the calculated, zero roughness, Fresnel reflectivity.

The interfacial tensions can also be measured with macroscopic techniques. The spinning drop technique is usually required to measure the very low tensions of microemulsion systems. We did not make independent, macroscopic measurements of the tensions. However, our values can be compared with macroscopic measurements available in the literature. Here we list those measurements of which we are aware. For the C_6E_2-hexadecane-water system at 61 °C (two-phase region), $\gamma_{ow}\approx 1.3$ mN/m [31], comparable with our value of 1.0 ± 0.1 mN/m. For the same system at 36 °C (three-phase region), two measurements yield $\gamma_{om}\approx 0.33$ mN/m [31] and $\gamma_{om}\approx 0.39$ mN/m [32], also comparable with our value of 0.27 ± 0.03 mN/m. For the $C_{10}E_4$-tetradecane-water system at 33.3 °C (two-phase region), $\gamma_{ow}\approx 0.053$ mN/m [33], comparable with our value of 0.058 ± 0.009 mN/m. For the same system at 38 °C (three-phase region) only the experimental value for the oil-water interface is available, measured by extracting the oil and water phases and placing them in contact with each other. This value is $\gamma_{ow}\approx 0.026$ mN/m [33]. In comparing our value of $\gamma_{om}=0.033\pm 0.007$ mN/m to this last value of γ_{ow}, it should be noted that γ_{om} is expected to be lower than γ_{ow} in the three-phase region, although our value is slightly higher. Our values of the interfacial tension γ (see Table II), obtained from fits to the x-ray scattering data, agree reasonably well with these literature values. Since our fitting procedure was not constrained by the literature values, this agreement gives us confidence in the reliability of our data analysis.

These interfaces also span a wide range of interfacial roughness from 25 Å to 165 Å. The relative values of roughness for the samples can be determined qualitatively by the deviation of the measurements from the zero roughness, Fresnel reflectivity (see Fig. 9). For the roughest samples this deviation is seen to be large even very close to the wave-vector transfer for total reflection. As expected from capillary wave theory the interfacial tension and roughness are inversely correlated; the lower the tension the higher the roughness. Since the measured values of roughness are much larger than the dimensions of any of the molecules, our data cannot be explained by a simple molecular ordering at an essentially flat interface.

The differences in the values of roughness for different $C_{10}E_4$ samples at the same temperature of 38 °C are not fully understood. Since different thermistors were used with different samples, the actual temperatures could differ by as much as 0.3 °C, which would lead to slightly different phase

compositions and interfacial tensions. Also, as noted in Sec. II B, $C_{10}E_4$ microemulsions were substantially more difficult to equilibrate then the other two microemulsions—perhaps the $C_{10}E_4$ samples were not fully equilibrated. Note that C_4E_1, which was the easiest to equilibrate of the three microemulsions studied, had very reproducible data. These differences, however, do not alter the main conclusions of the study.

One of the important predictions of the Ginzburg-Landau theories of microemulsions is the presence of an oscillatory interfacial profile on the microemulsion side of the oil-microemulsion interface of the form $\sin(k_s z)\exp(-z/\xi_s)$, with $k_s = 2\pi/d_s$ [13]. This profile represents layering of microscopic oil and water regions separated by monolayers of surfactant. This is essentially the result of the bicontinuous structure within the bulk microemulsion being constrained by the boundary condition of the interface. As discussed in the Introduction, the interfacial oscillatory profile is predicted to have the same repeat distance d_s and correlation length ξ_s as the structure within the bulk microemulsion. We did not expect to detect this layering in the C_4E_1 and C_6E_2 systems because the structure within the bulk microemulsion phases of these systems is weak. However, the $C_{10}E_4$ system is known to have a well defined structure in the bulk, making it a good candidate to detect an oscillatory interfacial profile [9].

To test for the presence of this oscillatory profile we analyzed the data for the $C_{10}E_4$ system using both a nonoscillatory steplike intrinsic profile (also used for the C_4E_1 and C_6E_2 systems) and an oscillatory profile (Fig. 5). Comparison of results for these two profiles for the $C_{10}E_4$ system at 38 °C shows that the interfacial tensions are the same within error bars, while the roughness differs slightly. The corresponding fits are visually indistinguishable (only fits for the steplike profile are shown in the figure). This is easy to understand by noting that our data probe only the region to the left of the peak in $|\Phi(q)|$ shown in the inset of Fig. 5, and that a corresponding increase in diffuse scattering with Q_z is easily offset in the fits by increasing σ. Therefore, even though the resultant fitting parameters are slightly different for the two intrinsic profiles considered, our data do not provide a basis for favoring one profile over the other.

Although our analysis cannot either confirm or deny the presence of an oscillatory profile with a repeat distance and correlation length similar to those of the bulk microemulsion ($d_b = 191$ Å and $\xi_b = 97$ Å), our analysis rules out profiles with a repeat distance d_s greater than about 500 Å. This upper bound was obtained by repeating the fits to the data while progressively increasing the value of repeat distance d_s (each time, the correlation length ξ_s was set to $d_s/2$, consistent with Ref. [9]). For values of d_s less than about 400 Å, fits were visually indistinguishable, and the χ^2 value for the fits was nearly constant. For larger values of d_s, the fits consistently underestimated the specular peak and the diffuse scattering at larger β, and χ^2 was rapidly increasing.

In order to make a more definitive statement about the existence and form of the oscillatory profile, it would be necessary to extend the Q_z range of diffuse scattering and reflectivity measurements. This could not be done in our experiments because the large interfacial roughness of the $C_{10}E_4$ samples leads to a surface signal that quickly decays below the level of the background bulk scattering as Q_z increases. Improvement in the signal to noise ratio could be made by reducing the sample size and therefore reducing the background bulk scattering. However, at the roughness level of 160 Å, doubling the Q_z range of our measurements while preserving the same signal to noise ratio at the end of the range would require an impractical reduction of the background level by 8–9 orders of magnitude. Nevertheless, the upper bound that we were able to place on the profile oscillatory length d_s demonstrates that if a system with significantly smaller roughness (higher interfacial tension) and similar characteristic microemulsion lengths could be found, this experimental technique could be used to obtain detailed information on the interfacial structure.

VI. CONCLUSION

We used x-ray reflectivity and diffuse scattering to probe the structure of interfaces between oil-rich and microemulsion bulk phases and between oil-rich and water-rich phases in three-component microemulsion systems. Capillary wave theory combined with the distorted wave Born approximation was used to analyze the x-ray data and extract values of the two fit parameters, interfacial tension γ and roughness σ. The agreement between the fits and the measurements was very good for the measured ranges of γ and σ given by $0.03\ \text{dyn/cm} < \gamma < 1.4\ \text{dyn/cm}$ and $25\ \text{Å} < \sigma < 165\ \text{Å}$.

For the strongest surfactant ($C_{10}E_4$) microemulsion, we analyzed the data using both step function and oscillatory profiles for the oil-microemulsion interface. Due to the limited range of the momentum transfer **Q** of our measurements, we were not able to unambiguously distinguish between the step profile and the theoretical prediction for the oscillatory profile. However, we also considered oscillatory profiles with longer repeat distances and showed that our data exclude repeat distances greater then 500 Å. This demonstrates that, if a system with lower roughness and/or longer repeat distance could be found, this experimental technique could be used to obtain more detailed information on the microstructure of these interfaces.

ACKNOWLEDGMENTS

We acknowledge the assistance of Zhongjian Zhang and Zhengqing Huang in conducting the x-ray measurements. This work was supported by the donors of the Petroleum Research Fund administered by the ACS, UIC Campus Research Board, and the NSF Division of Materials Research. Brookhaven National Laboratory is supported by the U.S. Department of Energy.

APPENDIX: BACKGROUND SCATTERING FROM LOWER PHASE

Figure 3 illustrates scattering from the lower phase. The main beam is incident at the center of the interface, at point *O*, at the distance $L/2$ from the edge of the sample, and

makes angles α and α' with the horizontal in the upper and lower phase, respectively. The two scattered rays shown, *a* and *b*, are measured by the detector at the same angle β with respect to the horizontal. Ray *a* is scattered from the refracted beam at the horizontal distance ξ_a from point *O* and reenters the upper phase before leaving the sample. Ray *b* is scattered directly from the lower phase into the air, without reentering the upper phase. Angles α' and β' are related to angles α and β through Snell's law, which for small angles can be written in the form $\theta' = (\theta^2 - \theta_c^2)^{1/2}$, with $\theta = \alpha, \beta$. To express the total scattered intensity, we denote by $P(\chi)d\chi$ the probability per unit length that an x ray in the lower phase will be scattered into angle $d\chi$ around the direction making an angle χ with the refracted beam (χ equals $\alpha' + \beta'$ and $\alpha' + \beta$ for the rays *a* and *b*, respectively). Then, if I_0 is the intensity of the x-ray beam before entering the sample, the total scattering from the lower phase into $d\beta$ around β can be written as a sum of contributions of types *a* and *b*,

$$I_{\mathrm{sc}} = I_0 e^{-\mu_u L/2} T_{ul}(\alpha) \Bigg[T_{lu}(\beta') \int_0^{\xi_1} d\xi P(\alpha' + \beta') d\beta' \times e^{-\mu_l \xi (1+\alpha'/\beta')} e^{-\mu_u [L/2 - \xi(1+\alpha'/\beta')]} + \int_{\xi_2}^{L/2} d\xi P(\alpha' + \beta) d\beta \, e^{-\mu_l L/2} \Bigg]. \tag{A1}$$

Here, μ_u and μ_l are the absorption coefficients in the upper and the lower phase, related to the absorption lengths l_u and l_l, given in Table II, as $\mu_u = l_u^{-1}$ and $\mu_l = l_l^{-1}$. T_{ul} and T_{lu} are the Fresnel intensity transmission coefficients from upper to lower phase and vice versa, and angles $\alpha, \alpha', \beta, \beta'$ are assumed to be small. Distance ξ_1 is the largest value of ξ for which the scattering of type *a* can occur, while ξ_2 is the smallest ξ for which scattering of type *b* can occur. They are given by

$$\xi_1 = \frac{L}{2} \frac{\beta'}{\alpha' + \beta'}, \qquad \xi_2 = \frac{L}{2} \frac{\beta}{\alpha' + \beta}. \tag{A2}$$

Equation (A1) evaluates to

$$I_{\mathrm{sc}} = I_0 e^{-\mu_u L} T_{ul}(\alpha) \Bigg[T_{lu}(\beta') P(\alpha' + \beta') \frac{\beta \, d\beta}{\alpha' + \beta'} \times \frac{1 - \exp[-(\mu_l - \mu_u)(1 + \alpha'/\beta')\xi_1]}{\mu_l - \mu_u} + \left(\frac{L}{2} - \xi_2 \right) P(\alpha' + \beta) d\beta \exp[-(\mu_l - \mu_u) L/2] \Bigg]. \tag{A3}$$

It should be noted that scattering of type *a* is possible only for $\beta > \theta_c$, since for $\beta = \theta_c$, $\beta' = 0$. We measure the scattering probability $P(\chi)d\chi$ by raising the interface above the beam, so that the unscattered beam passes through the lower phase over the entire length of travel through the sample.

[1] G. Gompper and M. Schick, in *Self-Assembling Amphiphilic Systems, Phase Transitions and Critical Phenomena,* edited by C. Domb and J. Lebowitz (Academic Press, London, 1994).
[2] T. Tlusty, S.A. Safran, and R. Strey, Phys. Rev. Lett. **84**, 1244 (2000).
[3] R. Goetz, G. Gompper, and R. Lipowsky, Phys. Rev. Lett. **82**, 221 (1999).
[4] H. Leitao, M.M.T. da Gama, and R. Strey, J. Chem. Phys. **108**, 4189 (1998).
[5] T. Tlusty, S.A. Safran, R. Menes, and R. Strey, Phys. Rev. Lett. **78**, 2616 (1997).
[6] M. Kahlweit and R. Strey, Angew. Chem. Int. Ed. Engl. **24**, 654 (1985).
[7] M. Teubner and R. Strey, J. Chem. Phys. **87**, 3195 (1987).
[8] K.V. Schubert, R. Strey, S.R. Kline, and E.W. Kaler, J. Chem. Phys. **101**, 5343 (1994).
[9] T. Sottmann, R. Strey, and S.H. Chen, J. Chem. Phys. **106**, 6483 (1997).
[10] M.S. Laver, U. Olsson, H. Wennerström, and R. Strey, J. Phys. II **4**, 515 (1994).
[11] W. Jahn and R. Strey, J. Phys. Chem. **92**, 2294 (1988).
[12] A. Bernheim-Grosswasser, T. Tlusty, S.A. Safran, and Y. Talmon, Langmuir **15**, 5448 (1999).
[13] G. Gompper and M. Schick, Phys. Rev. Lett. **65**, 1116 (1990).
[14] X.-L. Zhou, L.-T. Lee, S.-H. Chen, and R. Strey, Phys. Rev. A **46**, 6479 (1992).
[15] D.D. Lee, S.H. Chen, C.F. Majkrzak, and S.K. Satija, Phys. Rev. E **52**, R29 (1995).
[16] J. Meunier, J. Phys. (France) Lett. **46**, L (1985).
[17] L.T. Lee, D. Langevin, and B. Farnoux, Phys. Rev. Lett. **67**, 2678 (1991).
[18] B.R. McClain *et al.*, Phys. Rev. Lett. **72**, 246 (1994).
[19] D.M. Mitrinović, Ph.D. thesis, University of Illinois at Chicago, 2000.
[20] M.L. Schlossman *et al.*, Rev. Sci. Instrum. **68**, 4372 (1997).
[21] J.D. Weeks, J. Chem. Phys. **67**, 3106 (1977).
[22] S.K. Sinha, E.B. Sirota, and S. Garoff, Phys. Rev. B **38**, 2297 (1988).
[23] M. Born and E. Wolf, *Principles of Optics* (Pergamon Press, Oxford, 1980).
[24] H. Tostmann *et al.*, Phys. Rev. B **59**, 783 (1999).
[25] C. Fradin *et al.*, Nature (London) **403**, 871 (2000).
[26] A. Braslau *et al.*, Phys. Rev. A **38**, 2457 (1988).
[27] D.K. Schwartz *et al.*, Phys. Rev. A **41**, 5687 (1990).
[28] M.K. Sanyal, S.K. Sinha, K.G. Huang, and B.M. Ocko, Phys. Rev. Lett. **66**, 628 (1991).
[29] G. Gompper and M. Schick, in *Self-Assembling Amphiphilic Systems, Phase Transitions and Critical Phenomena* (Ref. [1]), pp. 87–89.

[30] For the cutoff parameter r_0, only a wide range of acceptable values could be quoted. This is because the roughness σ depends on r_0 only weakly (logarithmically), and therefore small variations in σ lead to large variations in r_0.
[31] L.J. Chen, W.J. Yan, M.C. Hsu, and D.L. Tyan, J. Phys. Chem. **98**, 1910 (1994).
[32] O. Abillon, L.T. Lee, D. Langevin, and K. Wong, Physica A **172**, 209 (1991).
[33] T. Sottmann and R. Strey, J. Chem. Phys. **106**, 8606 (1997).